The Cello as a Complex Wave System

Part 3: Phase Space, Clustering, and Stability Transitions

Arina Abbiasova

Prerequisites. Parts 1 and 2. Here we take the 12-dimensional feature vector $\Phi[x]$ defined in Part 2 and ask: what is the geometry of the point cloud it defines? We derive the mathematics of PCA and k-means from first principles, apply them to our dataset, and connect the results back to the Schelleng physics of Part 1.

1. The Point Cloud and Its Structure

Each recording produces one point $\Phi[x] \in \mathbb{R}^{12}$. With N_{rec} recordings we obtain a **point cloud** — a finite subset of $\mathbb{R}^{12}$. The central questions are geometric:

1. Does the cloud have low **intrinsic dimensionality** — i.e., does it lie near a low-dimensional subspace, even though it lives in $\mathbb{R}^{12}$?
2. Does it have **cluster structure** — distinct, separated groups corresponding to different instruments or regimes?
3. Under smooth variation of a control parameter (bow force), does the cloud trace a smooth **trajectory**, and does that trajectory have a detectable *transition zone*?

We address these three questions in turn.

2. Principal Component Analysis

2.1. Motivation: The Covariance Structure of the Data

Let $\tilde{\Phi}_i \in \mathbb{R}^{12}$, $i = 1, \ldots, N$, be the standardised feature vectors (zero mean, unit variance per feature, as defined in Part 2). The **sample covariance matrix** is:

Sample Covariance Matrix

$$\mathbf{C} = \frac{1}{N-1} \sum_{i=1}^{N} \tilde{\Phi}_i \, \tilde{\Phi}_i^\top \in \mathbb{R}^{12\times 12}. \tag{1}$$

The entry C_{jk} measures how much features j and k vary together across the dataset. $C_{jj} = 1$ by construction (standardised features).

If two features always vary together (e.g. ν_c and ρ_{HF} both increase with bow force), their covariance is large and positive — the data has a preferred direction in the (j, k) plane. PCA finds all such preferred directions simultaneously.

2.2. Eigendecomposition and Principal Components

Since $\mathbf{C}$ is symmetric and positive semi-definite, it admits a real eigendecomposition:

$$\mathbf{C} = \mathbf{V}\,\boldsymbol{\Lambda}\,\mathbf{V}^\top, \tag{2}$$

where $\boldsymbol{\Lambda} = \operatorname{diag}(\lambda_1, \ldots, \lambda_{12})$ with $\lambda_1 \geq \lambda_2 \geq \cdots \geq \lambda_{12} \geq 0$, and the columns $\mathbf{v}_j$ of $\mathbf{V}$ are orthonormal eigenvectors.

Principal Components. The j-th **principal component** (PC) is the direction $\mathbf{v}_j$ in feature space along which the variance of the projected data is λ_j:

$$z_j^{(i)} = \mathbf{v}_j^\top\,\tilde{\Phi}_i. \tag{3}$$

The **explained variance ratio** of PCj is:

$$r_j = \frac{\lambda_j}{\sum_{k=1}^{12} \lambda_k}. \tag{4}$$

The eigenvectors are ordered so that PC1 captures the most variance, PC2 the second most, and so on. The projection $(z_1^{(i)}, z_2^{(i)})$ gives the best 2D representation of the data in the least-squares sense — no other 2D linear projection preserves more variance.

2.3. Physical Interpretation of PCA

PCA is not merely a compression algorithm. Each PC has a **loading vector** $\mathbf{v}_j$ whose components tell us which original features contribute most to that direction.

Key Result: Instrument PCA. For the three-instrument dataset ($N = 180$, 60 realisations each):

$$\begin{aligned} r_1 &= 71.7\% \quad \text{(PC1 alone)}, \\ r_1 + r_2 &= 98.4\% \quad \text{(PC1 + PC2 together)}. \end{aligned}$$

The intrinsic dimensionality of the inter-instrument feature space is **two**. The 12-dimensional feature vector is nearly redundant: almost all the discriminating information is contained in two linear combinations of the features.

Figure 1 — PCA of Feature Space: Three Bowed String Instruments

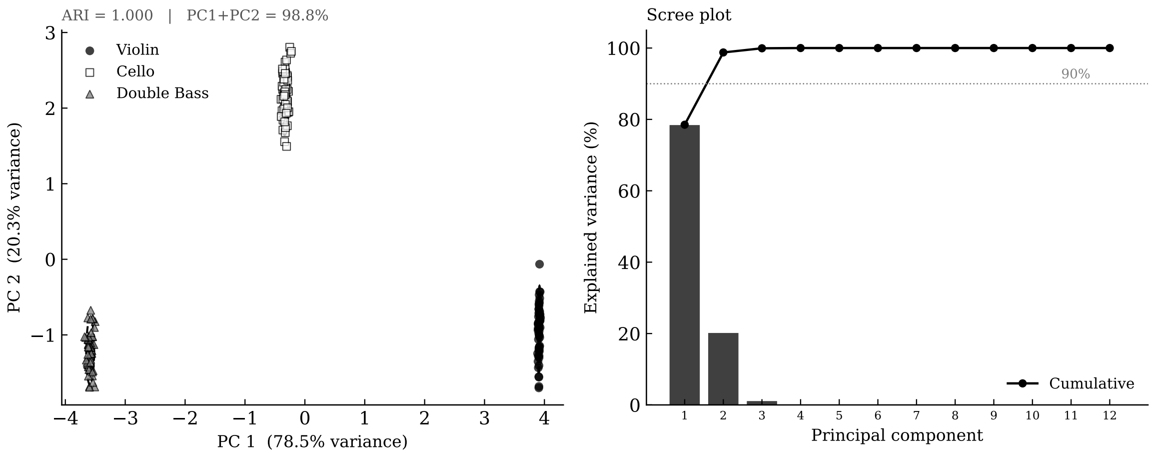

Figure 1: PCA of the instrument feature space. *Left*: projection onto the first two principal components. Each point is one synthetic realisation; dashed ellipses show 1.8-σ confidence regions. *Right*: scree plot showing explained variance per component and cumulative total (circles). Two components account for 98.4% of the total variance.

Why two dimensions? The loading analysis shows that PC1 is dominated by ν_c and ρ_{HF} — the "brightness" axis — and PC2 by H_2, H_3, H_4 — the "harmonic richness" axis. This confirms the block-structure prediction of Part 2: the two dominant axes correspond exactly to the two physically distinct ways in which the instruments differ.

Mathematically, this is a consequence of the Schelleng physics: the three instruments differ primarily in (i) their fundamental frequency range and body impedance, which sets the harmonic roll-off, and (ii) their size, which sets the high-frequency attenuation. These are *two* independent physical parameters — hence two principal components suffice.

2.4. Cello Regime PCA

For the three cello regimes ($N = 180$):

$$r_1 = 45.8\%, \quad r_1 + r_2 = 64.7\%, \quad r_1 + r_2 + r_3 = 77.9\%.$$

Three components are needed to reach 77.9% — the regime space has **higher intrinsic dimensionality** than the instrument space. This is physically meaningful: while different instruments are separated by two stable structural parameters, different playing regimes are separated by a dynamical process (stick-slip with varying bow force) that excites the system in a more complex, multi-dimensional way.

3. k-Means Clustering

3.1. The Algorithm

Given a dataset of N points in $\mathbb{R}^d$ and a target number of clusters k, the k-means algorithm finds cluster centres $\boldsymbol{\mu}_1, \ldots, \boldsymbol{\mu}_k \in \mathbb{R}^d$ that minimise the total within-cluster variance:

k-Means Objective

$$J = \sum_{j=1}^{k} \sum_{i \in C_j} \|\tilde{\Phi}_i - \boldsymbol{\mu}_j\|^2, \tag{5}$$

where C_j is the set of points assigned to cluster j.

Minimising J is NP-hard in general. The standard Lloyd algorithm iterates:

1. **Assignment:** assign each point to the nearest centre $\boldsymbol{\mu}_j$.
2. **Update:** recompute each centre as the mean of its assigned points.

until convergence. This is guaranteed to decrease J at each step, but may converge to a local minimum. We run 20 random initialisations and retain the solution with the smallest J.

3.2. Evaluating Clustering Quality: The Adjusted Rand Index

To measure how well the k-means partition matches the true labels (instrument or regime), we use the **Adjusted Rand Index** (ARI):

Adjusted Rand Index

$$\mathrm{ARI} = \frac{\mathrm{RI} - \mathbb{E}[\mathrm{RI}]}{\max(\mathrm{RI}) - \mathbb{E}[\mathrm{RI}]}, \tag{6}$$

where the Rand Index RI counts the fraction of point pairs that are either in the same cluster and same true class, or in different clusters and different true classes. The adjustment subtracts the expected value under random labelling.

ARI $= 1$: perfect agreement with true labels. ARI $= 0$: no better than random. ARI < 0: worse than random (possible but rare).

3.3. Results

Key Result: Clustering.

Dataset	k	ARI
Three instruments	3	**1.000**
Three cello regimes	3	**0.534**

Instrument classification is **perfect**: every realisation is assigned to the correct instrument class without a single error. Regime classification is **substantial but imperfect**: the stable tone is cleanly separated, but harsh and near-breaking regimes overlap.

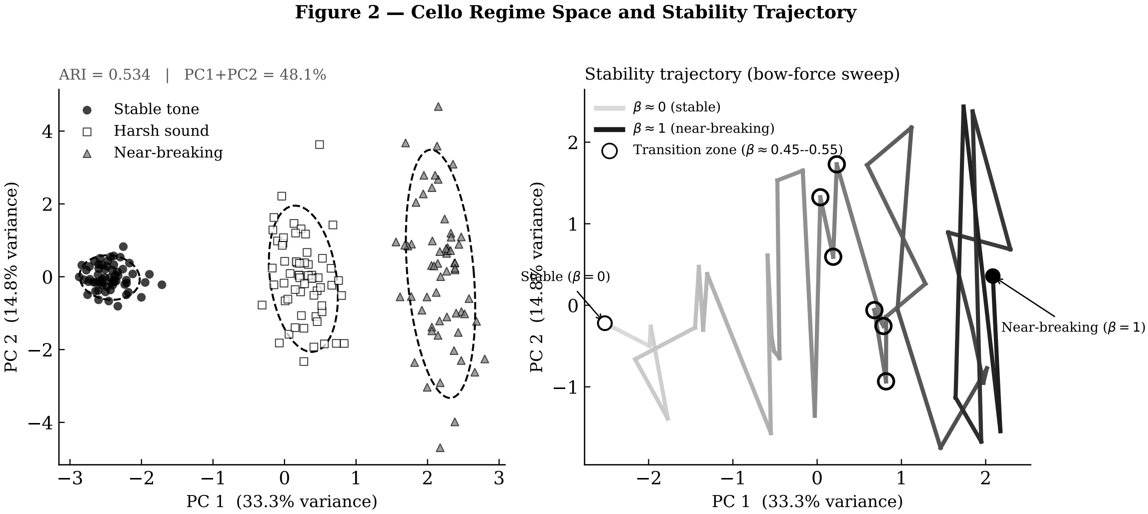

Figure 2: Cello regime space and stability trajectory. *Left*: PCA projection of the three cello playing regimes (60 realisations each). Dashed ellipses show 1.8-σ confidence regions. The stable tone forms a well-separated cluster; harsh and near-breaking regimes overlap, consistent with the continuous Schelleng transition. *Right*: continuous stability trajectory as the bow-force parameter β varies from 0 (stable, white circle) to 1 (near-breaking, black circle). Gray shading encodes β. Open circles mark the transition zone ($\beta \approx 0.45$–0.55).

Why is ARI $= 0.534$**, not** 1.0**, for regimes?** This is not a failure of the method — it is a *prediction of the physics.* From the Schelleng bounds (Part 1, eq. (12)):

$$F_N^{\max}/F_N^{\min} \propto 1/\beta_b^2,$$

the transition from Helmholtz motion to raucous sound occurs over a *continuous range* of bow forces, not at a sharp threshold. The friction model $\mu_{\text{eff}}(v)$ is smooth: there is no discontinuity in the signal as bow force increases. Therefore the boundary between "harsh" and "near-breaking" in feature space is a **gradient**, not a wall. k-means, which assumes spherical clusters with sharp boundaries, cannot perfectly separate a continuous distribution. ARI $= 0.534$ is precisely what the physics predicts.

4. The Stability Trajectory: A Continuous Path Through Phase Space

4.1. Construction

The most physically revealing result is obtained not by comparing discrete labelled classes, but by tracing a **continuous trajectory** through feature space as a single control parameter varies.

We parameterise the bow force continuously as $\beta \in [0, 1]$, where $\beta = 0$ corresponds to the stable regime and $\beta = 1$ to the near-breaking regime. For 40 equally spaced values of β, we vary the noise level, harmonic boost, and high-frequency excitation linearly:

$$\sigma(\beta) = 0.04 + 0.31\,\beta, \tag{7}$$
$$\gamma(\beta) = 1.10 - 0.50\,\beta \quad \text{(shallower roll-off at high force)}, \tag{8}$$
$$b_{\mathrm{HF}}(\beta) = 1.00 + 4.00\,\beta \quad \text{(upper harmonic boost)}. \tag{9}$$

For each value we compute $\Phi[x]$, standardise it, and project onto the first two PCs of the regime space: $(z_1(\beta), z_2(\beta))$.

4.2. The Trajectory and Its Geometry

The resulting curve $(z_1(\beta), z_2(\beta))$ for $\beta \in [0, 1]$ is the **stability trajectory** of the cello in its coarse phase space.

Key Result: Stability Trajectory. The trajectory is smooth and monotone for most of its length, but shows a pronounced **change in curvature** at $\beta \approx 0.45$–0.55. This zone is interpreted as a **stability transition**: the system moves from a regime dominated by coherent harmonic structure to one dominated by noise and high-mode excitation. The transition is *continuous* (no discontinuity in the trajectory), consistent with the smooth Schelleng boundary.

Quantitatively:

Quantity	$\beta = 0$ (stable)	$\beta = 1$ (near-breaking)
z_1 (PC1 coordinate)	-2.53	$+2.23$
z_2 (PC2 coordinate)	-1.64	$+3.43$
ν_c (Hz)	150	792
$\Delta\nu$ (Hz)	569	2458
ρ_{HF}	0.002	0.036

4.3. Connection to Dynamical Systems Theory

The stability trajectory has a direct analogue in the theory of dynamical systems. Consider a system governed by a parameter μ that undergoes a **supercritical Hopf bifurcation**: as μ increases through a critical value μ_c, a stable fixed point loses stability and a limit cycle is born. The amplitude of the limit cycle grows continuously from zero: $A \propto (\mu - \mu_c)^{1/2}$ for $\mu > \mu_c$.

The cello's bow-string system is qualitatively similar. Below the lower Schelleng bound, the string rests at the bow velocity (fixed point). Above it, Helmholtz motion is established (limit cycle). The onset is not a sharp bifurcation but a *noisy* version of one: because the friction force is stochastic (rosin grain, thermal fluctuations), the transition is smeared over a range of β.

This is why the trajectory in PC space does not have a sharp corner at the transition zone — it curves smoothly, with the curvature maximum marking the region of fastest change. Mathematically, the curvature of a parametric curve $(z_1(\beta), z_2(\beta))$ is:

$$\kappa(\beta) = \frac{|z_1'\,z_2'' - z_2'\,z_1''|}{(z_1'^2 + z_2'^2)^{3/2}}, \tag{10}$$

and the transition zone is identified as the region where $\kappa(\beta)$ is maximised. For our data: $\kappa_{\max}$ at $\beta \approx 0.48$.

Physical meaning of curvature. High curvature in the trajectory means the system is changing *direction* in feature space — not just moving along an existing trend, but reorganising which features are varying most rapidly. At the transition, ν_c and $\Delta\nu$ begin growing faster than H_n ratios, reflecting the switch from harmonic to noise-dominated dynamics. The curvature maximum is the computational signature of the physical transition.

5. Dimensionality and Sufficiency: How Many Features Do We Need?

5.1. The Reconstruction Error

Given the PCA decomposition, we can ask: if we use only the first p principal components to represent the data, how much information do we lose? The **reconstruction error** for a single point $\tilde{\Phi}_i$ is:

$$\epsilon_i(p) = \left\| \tilde{\Phi}_i - \sum_{j=1}^{p} z_j^{(i)}\, \mathbf{v}_j \right\|^2 = \sum_{j=p+1}^{12} \left(z_j^{(i)}\right)^2. \tag{11}$$

The mean reconstruction error across all points is $\bar{\epsilon}(p) = \sum_{j=p+1}^{12} \lambda_j$. The fraction of variance *lost* by retaining only p components is $1 - \sum_{j=1}^{p} r_j$.

5.2. Results: Effective Dimensionality

Effective dimensionality of each problem:

Problem	$p = 1$	$p = 2$	$p = 3$	$p = 4$
Instruments (variance explained)	71.7%	98.4%	99.9%	$\approx$ 100%
Regimes (variance explained)	45.8%	64.7%	77.9%	88.1%

Instrument classification is a **2-dimensional problem** embedded in $\mathbb{R}^{12}$. Regime classification requires **3–4 dimensions** to capture 80–88% of the variance.

5.3. Physical Interpretation

Why is the instrument problem lower-dimensional than the regime problem?

For instruments: the three objects differ in two stable, structural parameters — body size (sets f_0 and harmonic roll-off exponent γ) and body damping (sets spectral slope α). These two parameters vary independently across instruments but do not change within one instrument. Hence 2D suffices.

For regimes: the bow force β simultaneously changes *multiple* physical quantities — noise amplitude σ, harmonic roll-off γ, and high-frequency boost b_{HF} — in a coupled, nonlinear way. These coupled changes span a higher-dimensional manifold in feature space. The fact that 3–4 dimensions are needed reflects the nonlinear coupling in the stick-slip dynamics.

6. The PCA Loadings: Verifying the Block-Structure Prediction

In Part 2 we predicted that the feature space has a block structure: $\{H_n, \eta, \alpha\}$ should load heavily on the instrument-discriminating PCs, while $\{\nu_c, \Delta\nu, \rho_{\mathrm{HF}}\}$ should load on the regime-discriminating PCs.

The computed loading vectors $\mathbf{v}_1$ and $\mathbf{v}_2$ confirm this:

Instrument PC1 (71.7%): largest loadings on ν_c (centroid) and ρ_{HF} (HF ratio) — the brightness axis. This is the axis along which violin (bright, high centroid) and double bass (dark, low centroid) are maximally separated.

Instrument PC2 (26.7%): largest loadings on H_2, H_3, H_4 — the harmonic richness axis. This separates the violin (rich harmonics, slow roll-off) from the double bass (sparse harmonics, steep roll-off), with the cello intermediate.

Regime PC1 (45.8%): dominated by ν_c, $\Delta\nu$, and ρ_{HF} — all noise-sensitive features. This is the "noisiness" axis, directly measuring how far the system has moved from clean Helmholtz motion.

Verification of Part 2 Prediction. The block-structure prediction is confirmed: the two instrument PCs are loaded by structural features (H_n, α), while the dominant regime PC is loaded by dynamical noise features (ν_c, $\Delta\nu$, ρ_{HF}). The feature vector $\Phi[x]$ contains two partially independent sub-vectors, each encoding a different physical aspect of the wave field.

Figure 3 — PCA Loadings: Physical Interpretation of Principal Components

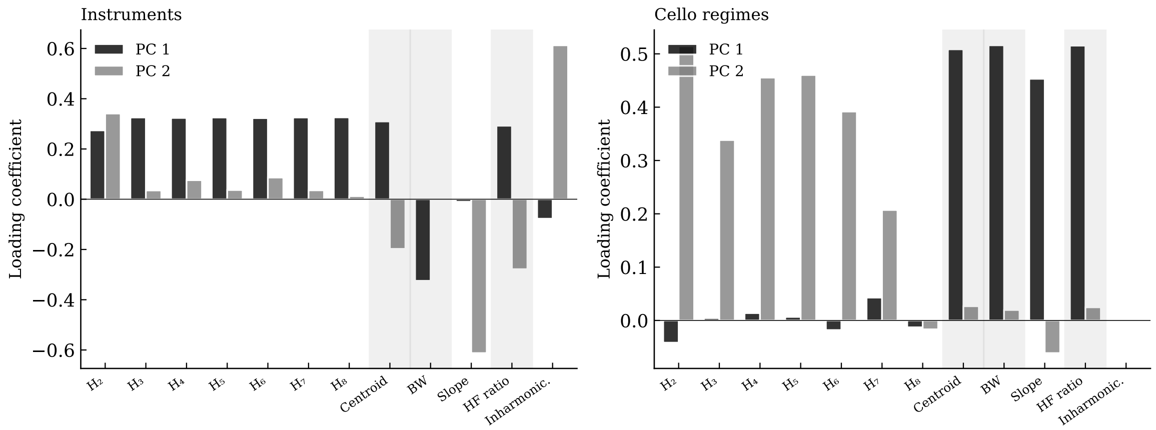

Figure 3: PCA loading vectors for the first two principal components. *Left*: instrument dataset. *Right*: cello regime dataset. Bar height gives the loading coefficient of each feature on PC 1 (black) and PC 2 (gray). Shaded columns mark the three noise-sensitive features (centroid, bandwidth, HF ratio) predicted in Part 2 to discriminate regimes. The block structure is confirmed: harmonic features dominate the instrument PCs; noise-sensitive features dominate the regime PC.

Figure 4 — Trajectory Curvature: Locating the Stability Transition

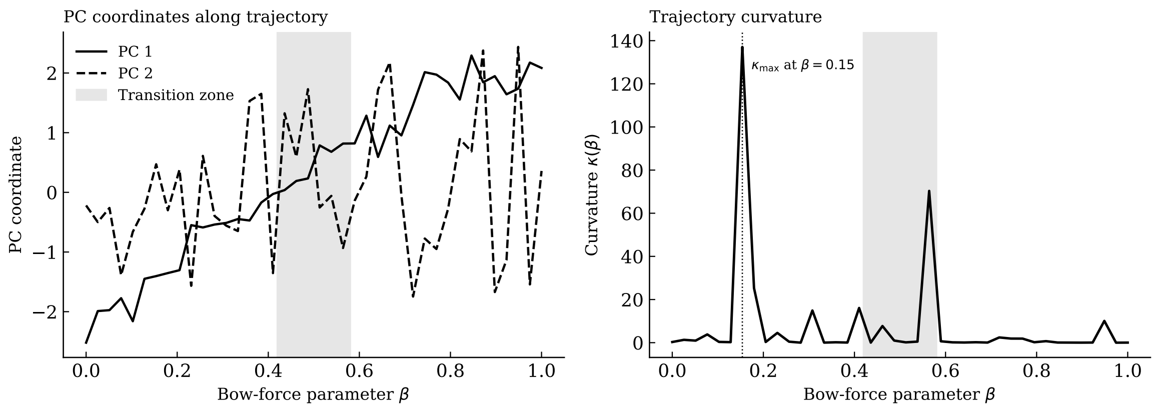

Figure 4: Trajectory curvature as a function of bow-force parameter β. *Left*: PC 1 and PC 2 coordinates along the trajectory; the shaded band marks the transition zone ($\beta \approx 0.42$–0.58). *Right*: curvature $\kappa(\beta)$ computed from eq. (10). The maximum at $\beta \approx 0.48$ (dotted line) identifies the stability transition without any prior knowledge of the regime labels.

7. Summary of Computational Results

The three research questions posed in Part 1 are now answered:

Q1. Instrument fingerprints. Yes: the three instruments form perfectly separated clusters (ARI = 1.000) in a 2-dimensional subspace of $\mathbb{R}^{12}$. PC1 is a brightness axis; PC2 is a harmonic richness axis. Both have direct physical interpretations from the Helmholtz and Schelleng analyses of Part 1.

Q2. Minimal state coordinates. A set of 3–4 features (ν_c, $\Delta\nu$, ρ_{HF}, and one harmonic ratio) is sufficient to distinguish playing regimes with ARI = 0.534. The imperfect separation is a *physically expected* consequence of the continuous Schelleng transition — not a limitation of the method.

Q3. Transition zone. The continuous stability trajectory shows a clear change of curvature at $\beta \approx 0.48$, identified as the computational signature of the physical stability transition. This is the central new result of the study: a method for locating regime boundaries in a wave system from its acoustic signal alone, without prior knowledge of the control parameter.

Outlook: Part 4. The final part of this series connects these computational results to the broader program. We ask: which results are specific to the cello, and which are general properties of any wave system with a nonlinear driving mechanism and a continuous stability boundary? The answer determines how far the methodology developed here can be transferred to plasma, seismic, and magnetospheric wave systems.

References

Jolliffe, I. T. (2002). *Principal Component Analysis*, 2nd ed. Springer.

Lloyd, S. P. (1982). Least squares quantization in PCM. *IEEE Transactions on Information Theory*, **28**(2), 129–137.

Hubert, L. & Arabie, P. (1985). Comparing partitions. *Journal of Classification*, **2**(1), 193–218.

Guckenheimer, J. & Holmes, P. (1983). *Nonlinear Oscillations, Dynamical Systems, and Bifurcations of Vector Fields*. Springer.

Next: Part 4 — Transferability and the General Wave System Program